

SC42030 Control for high resolution imaging

Homework Assignment 4 : Wavefront corrector and Coherence of light

Ali Nawaz

August 27, 2018

1 Focal length of GRIN lens

Gradient index (GRIN) lens are cylindrical lenses, where the refractive index n varies in the direction perpendicular to the optical axis. General expression for the refractive index of GRIN lens is described by Equation 1[2][3].

$$N = N_0 \cdot \left[1 - \frac{k}{2}r^2\right] \quad (1)$$

Where, N is the refractive index. N_0 is the base index at the center of lens
 k is the gradient constant and r is the variable radius [mm].

The given GRIN lens has a diameter of 1mm and the refractive index is outlined with the aid of expression: $n(r) = 1.6 - 0.5r^2$. The lens have a thickness of 0.1mm. This can be outlined in accordance with Equation 1, to the expression shown in Equation 2.

$$N = 1.6\left(1 - \frac{1}{1.6} \frac{1}{2}r^2\right) \quad (2)$$

Thus, $k = \frac{1}{1.6}$ and $N_0 = 1.6$

One might be tempted to conclude that the focal length of the GRIN lens is ∞ , since the radius of curvature is ∞ , in accordance with simple lens maker equation. However, this is incorrect. The varying refractive index n makes the GRIN lens to bear a finite focal length. The focal length and back focal length of a GRIN lens can be expressed as shown in Equation 3[2][3].

$$f = \frac{1}{N_0\sqrt{k} \sin(t\sqrt{k})}$$
$$\text{bfl} = f \cos(t\sqrt{k}) \quad (3)$$

In the above expression, f = focal length [mm], bfl = back focal length [mm]

t = GRIN lens thickness [mm].

Combining Equations 2 and 3. The focal length and backfocal length for the given GRIN lens is outlined in Equation 4.

focal length of the GRIN lens:

$$f = \frac{1}{1.6\sqrt{\frac{1}{1.6}} \sin\left(0.1 \cdot \sqrt{\frac{1}{1.6}}\right)}$$

$$f = 10.0104 \text{ [mm]}$$

The back focal length of the GRIN lens is:

$$\text{bfl} = f \cos\left(t\sqrt{k}\right)$$

$$\text{bfl} = 10.0104 \cos\left(0.1\sqrt{\frac{1}{1.6}}\right) = 9.9792 \text{ [mm]}$$

(4)

2 LC corrector

A given transmissive LC corrector is fabricated with a $20\mu m$ thick LC layer. The objective is to achieve a full 2π wavefront control. The LC material has a birefringence of $\Delta n = 0.15$. The maximum wavelength at which full 2π control can still be achieved is outlined in Equation 5[1].

A thin layer LC, serving as phase modulator, with phase modulation $\Delta\phi$ can be expressed as:

$$\Delta\phi = \frac{2\pi\Delta nt}{\lambda}$$

For 2π control this can be expressed as:

$$\lambda = \Delta nt$$

$$\lambda = 0.15 \cdot 20\mu m = 3\mu m$$

(5)

Now, the objective is to estimate the thickness of LC layer to achieve 2π wavefront control at a wavelength of $\lambda = 1.06\mu m$. Using the expressions from Equation 5, this is estimated in Equation 6[1].

$$\lambda = \Delta nt$$

$$1.06\mu m = 0.15 \cdot t$$

Thus, the thickness of the LC layer can be estimated as:

$$t = \frac{1.06 \cdot 10^{-6}}{0.15} = 7.0667\mu m$$

(6)

3 Membrane DM, Piezo Electric bimorph DM and continuous face-plate DM comparison

This section aims at comparing the advantages and disadvantages of different deformable mirrors, for an application requiring feedforward control. Three advantages and disadvantages are listed for each type.

Membrane DM

Advantages:

- Use of electrostatic or magnetic field for membrane deformation.
- Low voltage consumption and zero hysteresis.
- Ability to accommodate hundreds of actuators.

Disadvantages:

- Only pull actions are possible unless the membrane has to be pre-loaded for push action.
- Non linear behaviour due to force induced by electrostatic or magnetic field.
- Limited stroke length due to the inherent property of electrostatic/magnetic field used.

Piezoelectric bimorph DM

Advantages:

- Ease of control, both push-pull support by piezo actuator electrodes.
- Good reproduction of low-order Zernike modes and low amplitude of correction for higher order modes[1].
- Large stroke and reasonable time lead with great accuracy¹

Disadvantages:

- Considerable hysteresis present.
- High driving voltage and peak currents.
- High actuator price and low reliability.

Due to the hysteresis property feedback control is required to correct for the mirrors loss in precision.

Piezoelectric continuous faceplate DM

Advantages:

- Ease of implementation due to simple design, can be modelled with mechanical spring system.
- Plate edge moments for error-free correction of statistically important smooth low-order aberrations.
- Availability of custom design.

Disadvantages:

- About 2% hysteresis.
- Cross talk issues. Zero cross talk, mirror cannot be used for wavefront correction. Presence of cross talk if actuator stiffness is higher than faceplate stiffness.
- Hard to ensure stress free assembly of deformable plate and minimize coating stress.

4 Telescope aperture and actuator design

The objective is to observe through a frozen turbulent atmosphere with Fried parameter $r_0 = 7\text{cm}$ and wind velocity $\tau = 2\text{m/s}$. Membrane DM with 19 control channels, including tip-tilt is used.

First the required aperture/diameter of the telescope is estimated. To estimate this, the relation between Strehl ratio, relative actuator density $\frac{d_t}{r_0}$ and control bandwidth $\frac{f_G}{f_c}$ is used[1][Fig.6.7, pg-92]. A Strehl ratio of 0.85 is used. Corresponding relative actuator density has a value of 0.6. From this, the actuator spacing d_t can be obtained. Which in turn can be used to obtain aperture/telescope diameter D_t , since the total number of actuators is known, $N_a = 19$. The aperture diameter is estimated as shown in Equation 7[1].

¹Overview of Deformable Mirror Technologies for Adaptive Optics and Astronomy:
<https://www.eso.org/sci/libraries/SPIE2012/8447-05.pdf>

$$\frac{d_t}{r_0} = 0.6$$

$$d_t = 0.6 \cdot 7 \text{ cm}$$

$$d_t = 4.2 \text{ cm}$$

The diameter of the aperture can be estimated as:

$$N_a = \frac{\pi}{4} \cdot \left(\frac{D_t}{d_t} \right)^2 \quad (7)$$

$$19 = \frac{\pi}{4} \cdot \left(\frac{D_t}{4.2} \right)^2$$

Thus the aperture diameter is:

$$D_t = 20.65766 \text{ cm}$$

As a second step, the correction frequency is estimated. For the chosen Strehl ratio of 0.85, the control bandwidth $\frac{f_G}{f_c}$ is 0.15. To estimate the correction frequency f_c , first the Greenwood frequency f_G must be obtained. Greenwood Frequency can be estimated as shown in Equation 8[1].

Using Marechal approximation of Strehl ratio can be expressed in terms of phase variance:

$$S \approx e^{-\sigma_{phi}^2}$$

Phase variance due to delay can be expressed as:

$$\sigma_{delay}^2 = 28.44(f_G \tau)^{\frac{5}{3}} \quad (8)$$

$$\ln(1/S) = 28.44(f_G \tau)^{\frac{5}{3}}$$

$$\ln(1/0.85) = 28.44(f_G \cdot 2)^{\frac{5}{3}}$$

$$f_G = 0.02255 \text{ Hz}$$

Using the Greenwood frequency, the correction frequency can be obtained as outlined in Equation 9.

$$\begin{aligned} \frac{f_G}{f_c} &= 0.15 \\ f_c &= \frac{0.02255}{0.15} = 0.150336 \text{ Hz} \end{aligned} \quad (9)$$

For the final step, the maximum stroke required for optimal correction is estimated with the aid of total actuator stroke variance σ_{stroke}^2 . This is expressed in Equation 10. Wavelength $\lambda = 550\text{nm}$, is used for total stroke correction.

$$\sigma_{stroke}^2 = 1.03 \left(\frac{D_t}{r_0} \right)^{\frac{5}{3}}$$

$$\sigma_{stroke} = 2.50 \text{ rad}$$

Total piston stroke size can be expressed as: (10)

$$\text{Total piston stroke:} = \frac{5\sigma}{2} \cdot \frac{\lambda}{2\pi}$$

$$\text{Total piston stroke:} = \frac{5 \cdot 2.50}{2} \cdot \frac{550 \cdot 10^{-9}}{2\pi} = \pm 547.095 \text{ nm}$$

5 Aberration evaluation and mirror deflection estimation

First the aberrations observed in Figure 1[1][Figure 6.17] are identified.

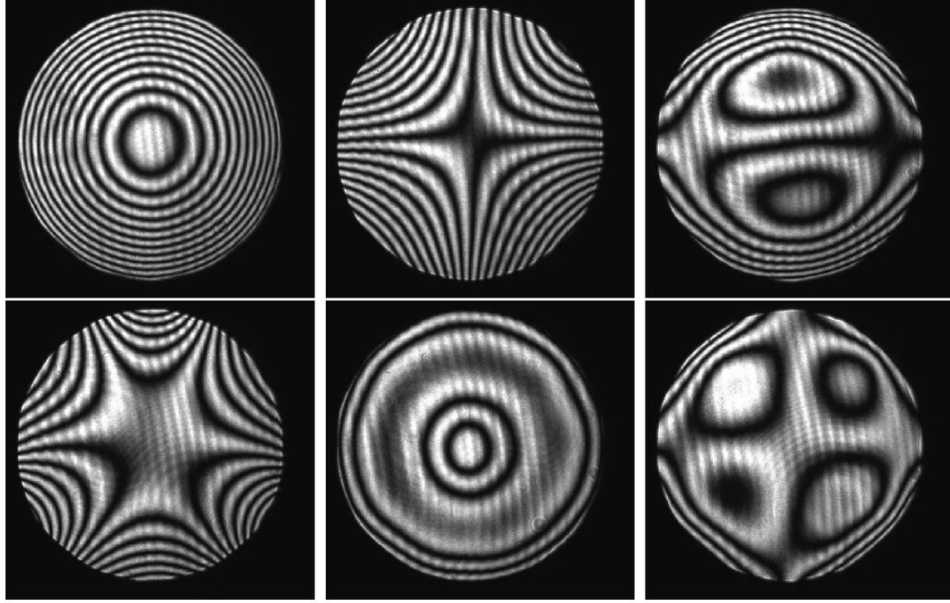


Figure 1: Interferograms of low order Zernike polynomials. Produced with a 37-ch piezoelectric DM.

The aberrations are simulated for verification. The script is provided in Section 10. The results of simulation are outlined in Figures 2-7. The captions indicate the respective interferogram from Figure 1. Images are ordered from left to right and then top to bottom. First image is the top left image, fourth image is the bottom left image and sixth image is the bottom right image.

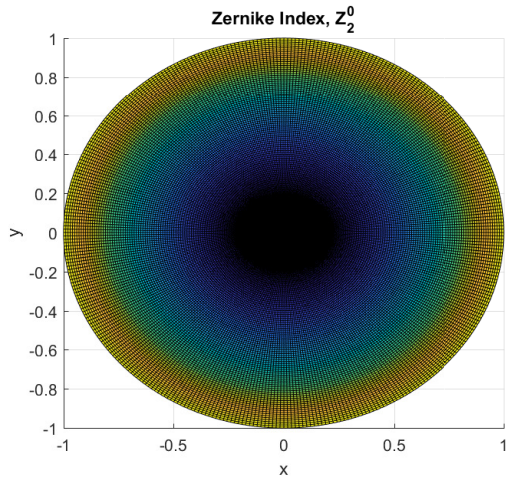


Figure 2: First image simulation, defocus aberration. Noll's ordering 4.

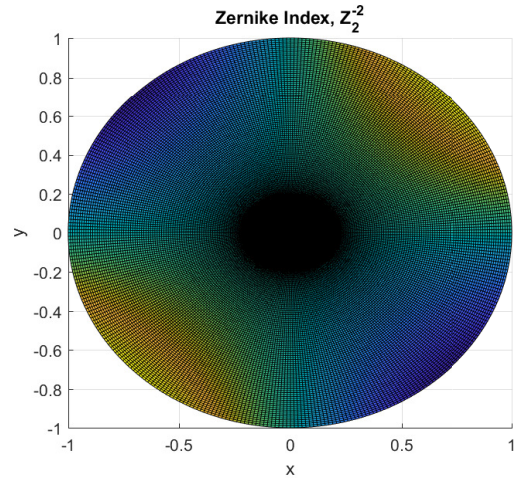


Figure 3: Second image simulation, astigmatism aberration. Noll's ordering 6.

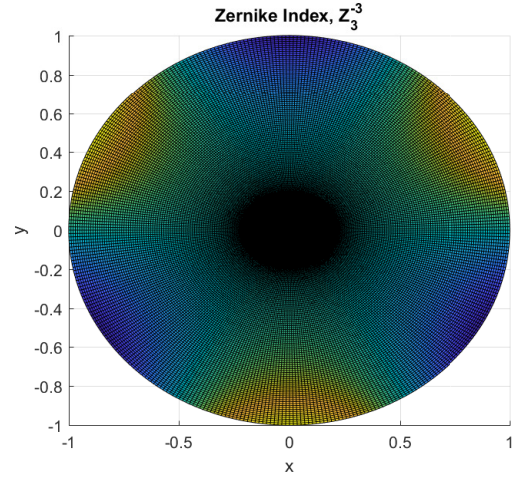
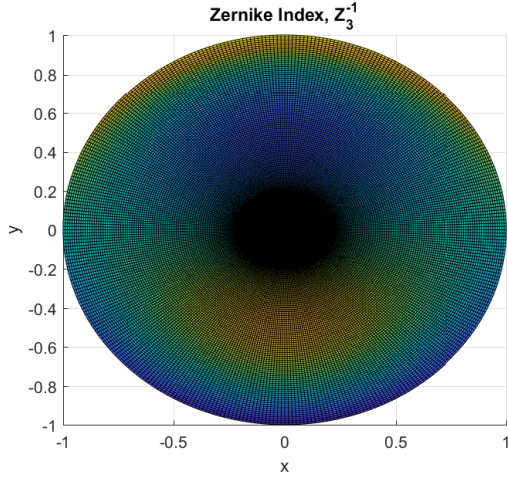


Figure 4: Third image simulation, coma aberration. Figure 5: Fourth image simulation, trefoil aberration. Noll's ordering 8.

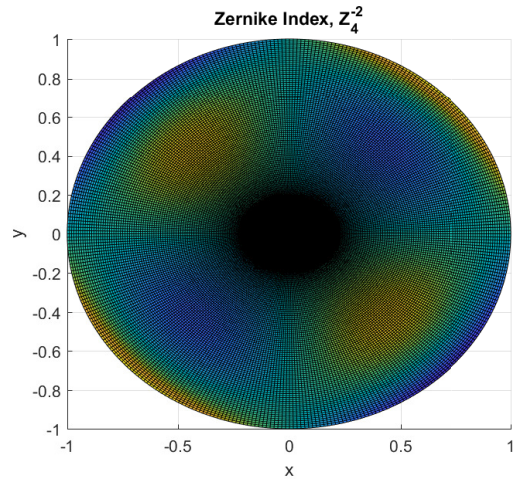
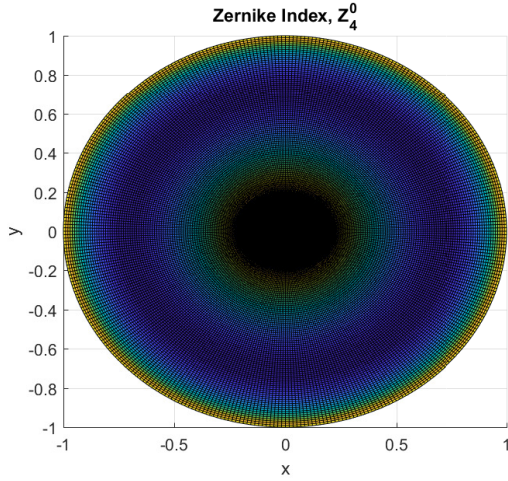


Figure 6: Fifth image simulation, spherical aberration. Noll's ordering 11. Figure 7: Sixth image simulation. Noll's ordering 13.

The magnitude of mirror deflection required to correct each of the aberrated wavefront needs to be half of the magnitude of the wavefront unflatness. Since the deflection distance of the mirror is travelled twice[1][Figure 6.1]. Each actuator should thus be capable of deflecting by an amount of $\frac{\lambda}{2}$, to cover an entire wavelength. For He-Ne laser, i.e. for $\lambda = 632.8 \text{ nm}$ ², the mirror deflection should be $\frac{632.8}{2} \text{ nm} = 316.4 \text{ nm}$. This multiplied with the aberration wavefront in Figures 2-7, would result in the respective mirror deflection shape for each aberration. Since the aberration wavefronts have a magnitude between 0 and 1.

6 Wavefront corrector design based on Alvarez principle

A wavefront corrector based on Alvarez principle, made of BK7 glass($n=1.5$)³ is constructed. The wavefront corrector produces 0 aberration at 0 shift. And it acts as a lens with focal length 2m when the

²He-Ne laser wavelength: https://www.rp-photonics.com/helium_neon_lasers.html

³BK7 glass refractive index <http://www.glassdynamicsllc.com/bk7.html>

components are shifted by $\delta = 0.5$ mm. First the radius of curvature R , for the curved side of the lens is estimated using the lens maker's Equation, in Equation 11.

$$\frac{1}{f} = (n - 1) \cdot \left(\frac{1}{R_1} - \frac{1}{R_2} \right)$$

Since, one side of the lens has ∞ radius of curvature, the expression becomes:

$$f = \frac{R}{n - 1}$$

$$R = f(n - 1) = 2(1.5 - 1) = 1 \text{ m}$$
(11)

The wavefront function of each lens component can be expressed as shown in Equation 12[1].

For 1D wavefront with $R = 1$ can be expressed as:

$$F(x, y) = \frac{x^2 + y^2}{2 \cdot R} = \frac{x^2 + y^2}{2 \cdot 1}$$

The wavefront function $f(x, y)$ can be expressed as:

$$f(x, y) = \int \frac{F(x, y)}{\delta} dx = \int \frac{\frac{x^2 + y^2}{2 \cdot 1}}{0.5 \cdot 10^{-3}} dx$$

$$f(x, y) = 1000 \cdot \left(\frac{1}{3} x^3 + xy^2 \right)$$
(12)

The corresponding expression for optical surface that needs to be formed on the surface of the glass is obtained in Equation 13[1].

$$S(x, y) = \frac{f(x, y)}{n - 1}$$

$$S(x, y) = 1000 \cdot \left(\frac{1}{3} x^3 + xy^2 \right) \cdot \frac{1}{1.5 - 1} = 2000 \cdot \left(\frac{1}{3} x^3 + xy^2 \right) [m^3]$$
(13)

With the above mentioned surface equation, the wavefront corrector is expected to perform in line with the requirements.

7 Venus: temporal coherence length and time under different conditions

The angular diameter of Venus is 1 arc minute. A median observation wavelength of 550nm is assumed. The objective is to estimate the spatial coherence length δ along with temporal coherence length l and time τ for different cases.

The spatial coherence length, δ is obtained using Equation 14.

$$\delta < \frac{\lambda}{1 \cdot \frac{\pi}{10800}}$$

$$\delta < 0.0019m$$
(14)

For spectrum of solar light in the range 350 and 650 nm, the temporal coherence length and the coherence time can be estimated as shown in Equation 15.

Temporal coherence length:

$$l_c = \frac{\lambda^2}{\Delta\lambda}$$

$$l_c = \frac{(550 \cdot 10^{-9})^2}{(650 - 350) \cdot 10^{-9}} = 1.0083 \mu m \quad (15)$$

Corresponding temporal coherence time:

$$\tau = \frac{l_c}{c} = \frac{1.0083 \cdot 10^{-6}}{3 \cdot 10^8} = 3.3611 \cdot 10^{-15} s$$

If the light is pass through a red cut off filter with cut off filter at 600nm, solar light is now contained in the range 350 and 600 nm. Corresponding temporal coherence length and time is estimated with the aid of Equation 17.

Temporal coherence length:

$$l_{red} = \frac{\lambda^2}{\Delta\lambda}$$

$$l_{red} = \frac{(550 \cdot 10^{-9})^2}{(600 - 350) \cdot 10^{-9}} = 1.2100 \mu m \quad (16)$$

Corresponding temporal coherence time:

$$\tau_{red} = \frac{l_{red}}{c} = \frac{1.2100 \cdot 10^{-6}}{3 \cdot 10^8} = 4.0333 \cdot 10^{-15} s$$

If the light is pass through a blue cut off filter with cut off filter at 400nm, solar light is now contained in the range 400 and 650 nm. Corresponding temporal coherence length and time is estimated with the aid of Equation 17.

Temporal coherence length:

$$l_{blue} = \frac{\lambda^2}{\Delta\lambda}$$

$$l_{blue} = \frac{(550 \cdot 10^{-9})^2}{(650 - 400) \cdot 10^{-9}} = 1.2100 \mu m \quad (17)$$

Corresponding temporal coherence time:

$$\tau_{blue} = \frac{l_{red}}{c} = \frac{1.2100 \cdot 10^{-6}}{3 \cdot 10^8} = 4.0333 \cdot 10^{-15} s$$

8 Young's interferometer illuminated by Venus

A Young's interferometer made from 2 pinholes, illuminated by an extended monochromatic source, will produce observable fringes if the distance between the pinholes is smaller than the size of the coherence patch, δ [1]. A red bandpass filter is used with transmission in the window of 600nm to 650nm. It is assumed that Venus is observed under a median wavelength of 625nm. Similarly, a blue bandpass filter is used with transmission in the range 350 to 400 nm. A median wavelength of 375nm is assumed.

Equation 18 checks whether, fringes can be observed for the given pinhole distance. Venus is still assumed to have an angular diameter of one arc minute.

For red pass transmission filter:

$$\delta < \frac{\lambda}{\beta} = \frac{625 \cdot 10^{-9}}{\frac{\pi}{10800}} = 0.0021 m \quad (18)$$

For blue pass transmission filter:

$$\delta < \frac{\lambda}{\beta} = \frac{375 \cdot 10^{-9}}{\frac{\pi}{10800}} = 0.0013 m$$

Since the given pinhole distance of 1 mm is less than both of the above estimations, fringes should be observed in both cases. The number of fringes counted from the optical axis to one side of the interferometer for both of the cases are estimated in Equation 19.

For red pass transmission filter:

$$N \approx \frac{\lambda}{\Delta\lambda} = \frac{625}{650 - 600} = 12.5$$

For blue pass transmission filter:

$$N \approx \frac{\lambda}{\Delta\lambda} = \frac{375}{400 - 350} = 7.5$$
(19)

9 AO from space against AO from ground

Two identical AO systems with aperture of 100cm are considered. One is place on the ground for observing the satellite at a distance of 2000 km. The other one is placed on the satellite, at a distance of 2000 km, to observe the ground. It is assumed that all technical issues are resolved such that the system can perform a complete correction of all aberrations on the pupil. The goal is to find which AO system is more efficient and why?

Since both of the AO have the same dimension and configurations, it can be assumed that both of them have the same Fried parameter r_0 . The turbulence coherence time τ , the characteristic time for the turbulence to move over a distance τ , is described by $\tau = r_0/v$. Here, v is the wind velocity of the turbulent frozen atmosphere wrt to the observer. Greenwood frequency $f_G \propto \frac{1}{\tau}$. For a single frozen layer with wind velocity v it can be computed as $f_G = 0.427(v/r_0)$ [1]. Temporal error scales as a power law of the Greenwood frequency to controller sampling frequency f_s , according to the relation in Equation 20.

$$\sigma_{temp}^2 = a_t \left(\frac{f_G}{f_s} \right)^{\frac{5}{3}}$$
(20)

For a higher f_G , a higher f_s is required to achieve a lower error. Assuming a circular orbit of spacecraft around uniform Earth, the orbital velocity of the spacecraft is described in Equation 21.

$$V = \sqrt{\frac{\mu_{Earth}}{r}} = \sqrt{\frac{3.986 \cdot 10^{14}}{(6378 + 2000) \cdot 10^3}}$$

$$V = 6.8976 \cdot 10^3 \text{ m/s}$$
(21)

Assuming that the satellite is pointed accurately towards the ground station. Relative velocity of the turbulent frozen atmosphere is \approx the orbital velocity of the spacecraft. This means to achieve similar temporal error σ_{temp} , the AO on spacecraft must have a significantly higher f_s , due to high f_G . Thus the AO system on ground is more efficient then the one place on the spacecraft at 2000km.

10 Matlab Scripts

Following is the Matlab script for generating Zernike modes:

```
1 % Generate Zernike
2 rho = [0:0.01:1]; % Define the range of radial vector rho
3 theta = [0:pi/180:2*pi]; % Define the range of theta
4 [Z_mn, m_feas] = zernike(1, rho, theta); % Return Zernike polynomial values
5 % over a meshgrid, and the corresponding m values. Each page of Z_mn represents
```

```

6 % each feasible value of m
7
8 function [zer,m] = zernike(n, rho, theta)
9     % Function determinates the
10    % Takes in the index n, generates corresponding m automatically.
11    % Returns the Zernike matrices  $Z_{\{n\}^{\{+-m\}}(\rho, \theta)$ 
12    % # INPUT PARAMETERS: (n, rho, theta)
13    % * n, polynomial base index, generate +-m automatically.
14    % * rho, radial vector [0,1]
15    % * theta, angle vector [0, 2*pi] [rad]
16    % # OUTPUT PARAMETERS: [zer,m]
17    % * zer = Zernike Polynomial matrix over meshgrid of rho and theta,
18    %   rows and columns of meshgrid with values over pages. Each page
19    %   defines the m value. first matrix page = first m value.
20    % * m = m index
21    % * figures automatically generated
22    % # Author: Ali Nawaz
23    % * MSc student, "Space Exploration" and "Systems and Control Engineering"
24    % * Faculty of Aerospace Engineering, LR, Delft University of Technology.
25    % * Faculty of Mechanical, Maritime and Materials Engineering, 3ME Delft
26    %   University of Technology.
27
28    [rho,theta] = meshgrid(rho,theta); % generate meshgrid of rho and theta
29    [xbuf, ybuf] = pol2cart(theta, rho); % transform from cylindrical to cartesian ...
30    % co-ordinates
31    syms s; % symbol s for symbolic summation
32    m_list = [0:1:n]; % list of m to be selected from
33    Z_mn = []; % initialize Zernike [(:,:,page)] where organised in order of feasible m
34    m_feas = []; % select the feasible m
35
36    count = 0; % count the number of instances m is feasible
37    for k = 1:length(m_list)
38        if mod(n - m_list(k),2)==0
39            m_feas = [m_feas,m_list(k)]; % list feasible m
40            index1 = (n+m_list(k))/2;
41            index2 = (n-m_list(k))/2;
42            count = count +1;
43            % Find the corresponding radial polynomial
44            R_mn(:,:,count) = symsum( (((-1)^(s))*factorial((n-s)))/( ...
45                factorial(s)*factorial(index1 -s)*factorial(index2 - s) ) ...
46                ).*rho.^(n-2*s) , s,0, index2 );
47        end
48    end
49
50    % Extending m and R_mn to negative values of m
51    if mod(n,2) == 0
52        m_feas = [-m_feas(2:end),m_feas];
53    % Zernike polynomial values in form of meshgrid
54    Z_mn = cat(3,R_mn(:,:,2:end),R_mn);
55    elseif mod(n,2) == 1
56        m_feas = [-m_feas,m_feas];
57    % Zernike polynomial values in form of meshgrid
58    Z_mn = cat(3,R_mn,R_mn);
59    end
60
61    % Multiplication of azimuthal harmonic component of frequency
62    for q = 1:length(m_feas)
63        if m_feas(q) > 0
64            Z_mn(:,:,q) = Z_mn(:,:,q).*cos(abs(m_feas(q)).*theta);
65        elseif m_feas(q) < 0
66            Z_mn(:,:,q) = Z_mn(:,:,q).*sin(abs(m_feas(q)).*theta);
67        else
68            Z_mn(:,:,q) = Z_mn(:,:,q).*1;
69        end
70    end
71
72    zer = double(Z_mn); % final zernike polynomials in forms of meshgrids
73    m = m_feas; % final values of m
74
75    % Plot results

```

```

73     for r = 1:length(m.feas)
74         figure(r)
75         surf(xbuf, ybuf, zer(:, :, r))
76         title(['Zernike Index, Z-{' , num2str(n), '^{' , num2str(m.feas(r)), '}' ]]);
77         xlabel('x'),
78         ylabel('y')
79         zlabel('z')
80     end
81 end

```

References

- [1] MICHEL VERHAEGEN, PAULO POZZI, OLEG SOLOVIEV, GLEB VDOVIN, DEAN WILDING. *Control for High Resolution Imaging*. Lecture notes for the course SC42030 TU Delft, 2017.
- [2] RIEDL, M. J. *Optical Design Fundamentals for Infrared Systems, 2nd Edition*. SPIE - The International Society for Optical Engineering., 2001.
- [3] WARREN J. SMITH. *Modern Optical Engineering, 3rd Edition*. McGraw-Hill, 2000.